RSC Advances

Color-tunable luminescence and energy transfer properties of Eu2+ and Mn2+-activated BaCa2MgSi2O8 phosphor for ultraviolet light-emitting diodes

Journal:	*RSC Advances*
Manuscript ID:	RA-ART-11-2014-014848.R1
Article Type:	Paper
Date Submitted by the Author:	02-Jan-2015

Complete List of Authors:	Yang, Zheng; Northwest University, Institute of Photonics&Photon-Technology Northwest University Lin, Pin-Chun; Chung Yuan Christian University, Department of Chemical Engineering Guo, Chongfeng; Northwest University, Department of Physics Liu, Wei-Ren; Chung Yuan Christian University, Department of Chemical Engineering

RSC Advances RSCPublishing

PAPER

Color-tunable luminescence and energy transfer properties of Eu^{2+} and Mn^{2+}-activated $BaCa_2MgSi_2O_8$ phosphor for ultraviolet light-emitting diodes

Cite this: *RSC Advances*, 2015, xx, xx

Zheng Yang,[a] Pin-Chun Lin,[b] Chong-Feng Guo[a,*] and Wei-Ren Liu [b,*]

A color-tunable $BaCa_2MgSi_2O_8$:Eu^{2+}, Mn^{2+} phosphor (BCMSO:Eu,Mn) was synthesized by a solid state reaction. The BCMSO:Eu exhibits blue emission and broad excitation bands corresponding to the allowed f→d electronic transition of Eu^{2+}, which can match well with ultraviolet(UV) light emitting diode (LED) chips. In addition, via the design of efficient energy transfer from Eu^{2+} to Mn^{2+}, the emission hue could be controlled by tuning the Eu^{2+}/Mn^{2+} ratio and the emission hue of BCMSO:Eu,Mn varied from blue to while-light and eventually to red. Meanwhile, a high quality of white-emitting light could be generated in the optimized composition of BCMSO:1%Eu^{2+}, 20%Mn^{2+} with CIE coordinates of (0.3384, 0.2176) and CRI of 82, which is superior than that of blue chip and YAG phosphors. The results indicate that as-synthesized BCMSO:Eu^{2+}, Mn^{2+} phosphors exhibits the potential single-phased and UV excitable white-emitting phosphor.

Received 00th xx 2015,
Accepted 00th xx 2015

DOI: 10.1039/x0xx00000x

www.rsc.org/advances

1. Introduction

White light-emitting diodes (LEDs) are considered as a promising technology for next generation solid-state lighting systems because they are environmentally friendly and have several advantages such as long operation lifetime, energy saving capabilities and high material stability.[1-3] In order to obtain white LEDs, the major design choice includes two possibilities: one is color mixing, which involves a combination of trichromatic red-, green-, and blue-emitting LED chips.[4] The other is a very cheap way, phosphor down conversion, involving use of a blue chips combined with a yellow-emitting phosphor (cerium (III) doped yttrium aluminum garnet (YAG:Ce^{3+}))[5] or a blend of red-, green-, and blue-emitting phosphors pumped by ultraviolet (UV: 360-380nm)/near-ultraviolet (NUV: 380-420nm) chips.[6-7]

At present, commercial white LEDs based on the YAG:Ce^{3+} phosphor exhibit a poor color rendering index and a highly correlated color temperature due to the lack of a red light contribution. In addition, white-light LEDs can be easily fabrication by integrating red, green, and blue phosphors into a UV/NUV chip, but the disadvantages in this case are the high expenses, the trade-off luminescent efficiency, the fluorescence reabsorption, and the different attenuation situation of tri-color phosphors after being used for a period of time.

Therefore, to pursue efficient white LEDs, one of the strategies for generating different emission color from single-phased phosphors can be realized by co-doped sensitizer and activator into the same host and the existed energy transfer (ET) process will show interesting multi-color emission. Frequently , the effective way to acquire white light is to utilize the energy transfer from a sensitizer (Eu^{2+}, Ce^{3+} etc.) to a activator (Mn^{2+}, Tb^{3+}, Dy^{3+} etc.), which can be well accommodated in numerous hosts, owing to its good color reproducibility and low cost. Accordingly, many new single-phase phosphors for the UV white LEDs have been reported, such as $KCaY(PO_4)_2$: Eu^{2+}, Mn^{2+},[8] $BaMg_2Al_6Si_9O_{30}$:Eu^{2+},Tb^{3+},Mn^{2+},[9] $Ca_8MgGd(PO_4)_7$:Ln^{3+}, Mn^{2+} (Ln^{3+}=Ce^{3+}, Tb^{3+}, Dy^{3+}),[10] and so on.

Since the number of the existing silicate compounds in the inorganic phase database is large, great attention is also paid to the white-light silicate phosphors for the application in UV pumped LEDs, and some luminescence properties can be expected to be optimized.[11] Especially, silicates of $M_3MgSi_2O_8$(M=Ba, Sr, and Ca) have received recent attention because Eu^{2+}-and/or Mn^{2+}- doped powders have exhibited efficacy in white-light devices.[12] The structure of M_3=$BaCa_2$ was reported to have the $K_3NaS_2O_8$-type structure in the trigonal space group *P3*,[13-14] and Hou et al.[15-16] have reported the luminescence properties of Eu^{2+} doped $BaCa_2MgSi_2O_8$. It is expected that $BaCa_2MgSi_2O_8$: Eu^{2+} will have high luminescence

efficiency under NUV/UV excitation. At a later date, You et al.[17] further investigated the luminescent properties of Tb^{3+}/Mn^{2+} doped $BaCa_2MgSi_2O_8:Eu^{2+}$. However, up to now, the color-tunable $BaCa_2MgSi_2O_8:Eu^{2+}$, Mn^{2+} phosphors for UV-pumped white-light emitting diodes have not been reported.

Herein, we have demonstrated a novel tunable single-component white-light $BaCa_2MgSi_2O_8:Eu^{2+}$, Mn^{2+} phosphor for UV-light emitting diodes. The luminescent properties, the energy transfer from Eu^{2+} to Mn^{2+} ions and critical distances between them in this host have also been discussed in detail. Besides, the tunable emission color from blue to white and eventually to red has been realized through adjusting dopant concentration of Mn^{2+} at fixed Eu^{2+} content, which exhibit a good thermal stability and high quantum efficiency. The white LEDs fabricated based on $BaCa_2MgSi_2O_8:Eu^{2+}$, Mn^{2+} performed with good color-rendering index and high luminous efficacy. These results demonstrated that $BaCa_2MgSi_2O_8:Eu^{2+}$, Mn^{2+} is a great potential to be a color-tunable phosphor for UV chips excited white LEDs.

2. Experimental section

2.1. Sample preparation

The powder samples $BaCa_2MgSi_2O_8$(BCMSO): *x* Eu^{2+}, *y* Mn^{2+} were synthesized by a high temperature solid state reaction. The raw materials are analytical reagents $CaCO_3$, $BaCO_3$, MgO, SiO_2, Eu_2O_3 (99.99%), and MnO, two weight percent of NH_4Cl was used as a flux. The weighed powder was mixed in an agate mortar and placed in an alumina crucible. This crucible was heated at 1200°C for 8 h under a reducing atmosphere of 15%H_2/85%N_2. The final products were achieved in white powders after cooling to room temperature (RT).

2.2. Sample characterization

The crystal structure and phase purity of BCMSO: *x* Eu^{2+},*y* Mn^{2+} phosphors were carefully checked using powder X-ray diffraction (XRD) analysis (Bruker AXS D8) with CuK radiation (λ = 1.5418 Å) planes collected between 2θ = 10°–80° at 45 kV and 40 mA. The photoluminescence (PL) and photoluminescence excitation (PLE) spectra were measured using an Horiba Jobin-Yvon FluoroMax-4 spectrometer equipped with a 450 W xenon lamp as the excitation source. Time resolved measurements were performed using the Multi Channels Scaling (MCS) electronics NanoHarp 250 of the PicoQuant (PicoQuant GmbH, Germany), equipped with a PDL 800-B laser pulse driver. A pulsed laser diode LDH-396 (Lamda = 375 nm, pulse FWHM <70 ps, repetition rate 50 kHz – 40 MHz) was used to excite the sample and mounted directly on the sample chamber at room temperature.

3. Results and discussion

3.1. Crystal structure

The incorporation of Eu^{2+} and Mn^{2+} ions into the crystal lattice of BCMSO was examined by X-ray diffraction (XRD) analysis. Figure 1a and 1b present the XRD patterns of two typical samples $Ba_{0.99}Eu_{0.01}Ca_2MgSi_2O_8$ and $Ba_{0.99}Eu_{0.01}Ca_2Mg_{0.7}Mn_{0.3}Si_2O_8$. The diffraction patterns of all the samples are identical to each other, all peaks agree well with the Joint Committee on Powder Diffraction Standards (JCPDS) File No.31-0129 pattern. These results indicate that doping of Eu^{2+} and Mn^{2+} into BCMSO does not generate any impurity phase. Ivanov and Kirov[18] first reported the X-ray single crystal structure of BCMSO,which crystallizes in the orthorhombic system with eight formula units per unit cell. The dimensions of the unit cell are *a*=10.84Å, *b*=18.78Å, and *c*=6.77Å. Figure 1c shows a schematic of the BCMSO crystal structure and the environment of the Ba and Ca atoms, respectively.

The BCMSO crystal structure composed of MgO_6 octahedral, SiO_4 tetrahedra, BaO_{12} and CaO_7 polyhedra in the lattice. Three O atoms of a SiO_4 tetrahedron are used to connect three MgO_6 octahedral. There are two distinct crystallographic sites for alkali earth metal atoms[13]: Ba atom is twelve-fold coordinated by six O_2 and six O_1 atoms, and Ca atom is seven-fold coordinated by oxygen atoms. Base on the effective ionic radii(r) of cations with different coordination numbers (CN) reported by Shannon,[19] Eu^{2+} ions (r=1.45 Å when CN=12, r=1.20 Å when CN=7) can enter both Ba^{2+}(r=1.61Å when CN=12) and Ca^{2+}(r=1.06Å when CN=7) sites. Mn^{2+} ions should occupy the Mg^{2+} ion sites in the BCMSO host.

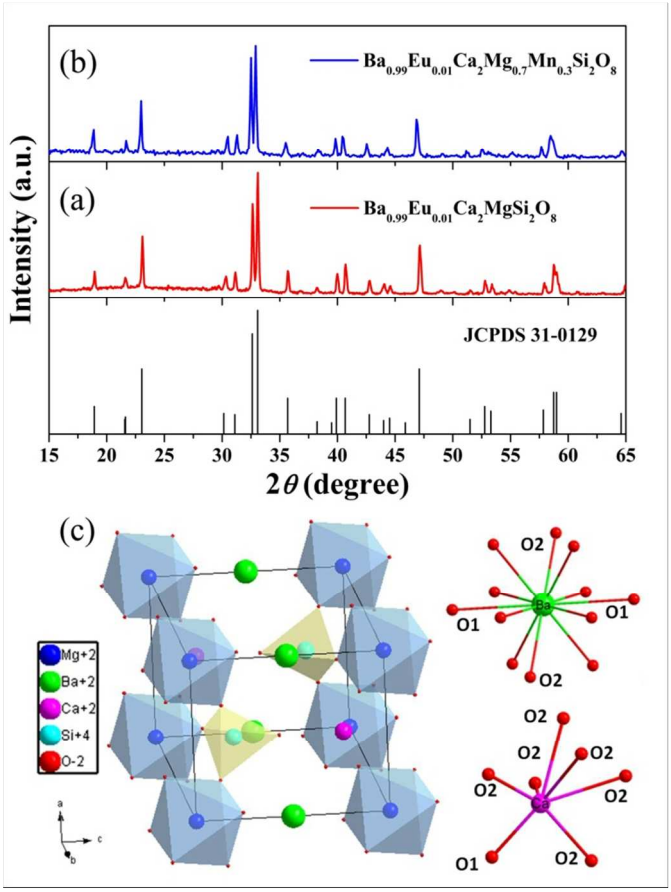

Fig. 1 Powder XRD patterns of (a) $Ba_{0.99}Eu_{0.01}Ca_2MgSi_2O_8$, (b) $Ba_{0.99}Eu_{0.01}Ca_2Mg_{0.7}Mn_{0.3}Si_2O_8$ and (c) the crystal structure of $BaCa_2MgSi_2O_8$ and coordination environment of Ba and Ca atoms in $BaCa_2MgSi_2O_8$.

3.2. Luminescence properties

The PLE (λ_{em}=446 nm) and PL (λ_{ex}=360 nm) spectra of $BaCa_2MgSi_2O_8$: *x* Eu^{2+} phosphors (*x*=0.01, 0.02, 0.04, 0.06, 0.08, 0.10, 0.12) are shown in Fig. 2. When monitored by the emission at 446nm , the PLE spectra show broad absorption bands ranging from 240 to 430nm with a maximum at 360nm, which is assigned to the parity allowed $4f^7(^8S_{7/2})\rightarrow 4f^65d$ transition of Eu^{2+} ions. Under the

excitation at 360nm, which represented the typical emission peak available in commercial LED chips, all the PL spectra presented a broad asymmetrical emission band from 390nm to 600nm with the emission peak at around 446nm. Asymmetrical emission characteristic may result from Eu^{2+} occupying both Ba^{2+} and Ca^{2+} sites.[15]

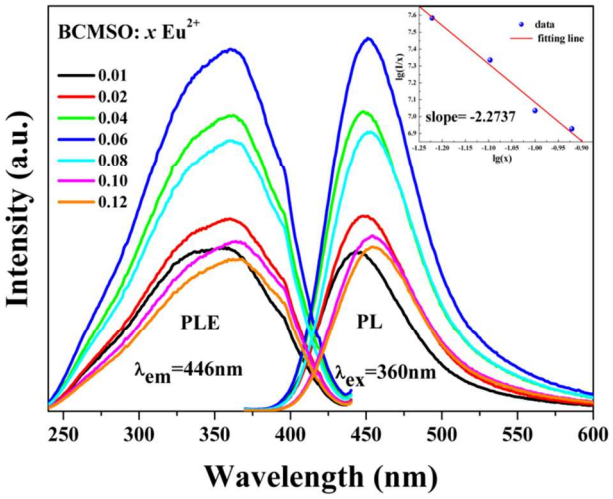

Fig. 2 PLE and PL spectra of $BaCa_2MgSi_2O_8$:$x$$Eu^{2+}$ phosphors (x=0.01, 0.02, 0.04, 0.06, 0.08, 0.10, 0.12), and the inset shows the fitting of log(I/x) vs log(x) in $BaCa_2MgSi_2O_8$:x Eu^{2+} phosphors.

The emission peak wavelengths of these phosphors vary with Eu^{2+} concentration, and there is a red shift in the emission wavelength with increasing Eu^{2+} concentration, which is presented in Fig. 3. The red shift was mainly ascribed to the lattice distortion resulting from the mismatch between larger Ba^{2+} (r=1.61Å, CN=12) and smaller Eu^{2+} (r=1.45 Å, CN=12) radii. On enhancing the amount of europium in the phosphor host, the lattice parameters of the host decreased leading to the crystal field strength increasing. Therefore, the emission shifts to a longer wavelength.[20] With gradual increase of Eu^{2+} doping concentration, we can see that the emission intensity of Eu^{2+} rises first until the maximum x at 0.06 and then drops, which can be explained by the increase of activator centersand then the appearance of concentration quenching effect when the distance between activators is close enough at high Eu^{2+} content, respectively. The intensity dependence of Eu^{2+} emission on various Eu^{2+} content are shown in Fig. 3.

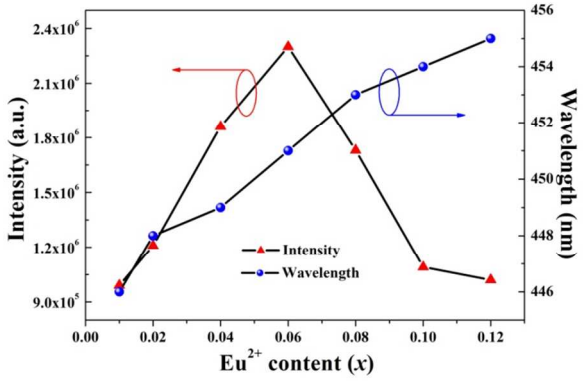

Fig. 3 The intensity and wavelength dependence of Eu^{2+} emission on the Eu^{2+} content x in samples $BaCa_2MgSi_2O_8$:x Eu^{2+}.

It is accepted that concentration quenching can be ascribed to the energy transfer between Eu^{2+} ions followed by energy transfer to traps or quenching sites. Therefore, in order to further confirm the process of energy transfer between Eu^{2+} ions in the BCMSO:Eu^{2+} phosphor, the interaction type between sensitizers or between the sensitizer and activator can be calculated by the following equation:[21]

$$I / x = k[1 + \beta(x)^{\theta/3}]^{-1} \qquad (1)$$

Where x is the activator concentration; I/x is the emission intensity (I) per activator concentration (x); k and β are constants for the same excitation condition; and θ is a function of multipole-multipole interaction. When the value of θ is 6, 8, or 10, it is the cause to say that the interaction form corresponds to dipole-dipole (d-d), dipole-quadrupole (d-q), or quadrupole-quadrupole (q-q), respectively. To get a correct θ value, the relationship between the lg(I/x) and lg(x) is plotted in the inset of Fig. 2. The slope of the straight line is $-\theta/3$=–2.2737. So, the value of θ can be calculated to be 6.8211, which is close to 6, indicating that in BCMSO:Eu^{2+} phosphors the quenching is dominated by the dipole-dipole interaction.

In order to investigate the concentration quenching phenomenon, the critical distance can be evaluated by the equation suggested by Blasse: [22]

$$R_C \approx 2\left[\frac{3V}{4\pi X_C N}\right]^{1/3} \qquad (2)$$

Where V is the volume of the unit cell, N is the number of host cations in the unit cell, and X_c is the critical concentration of dopant ions. For the BCMSO host, N=8, V=1378.2Å^3, and X_c is 0.06 for Eu^{2+}. Accordingly, the critical distance (Rc) was estimated to be about 17.63 Å. For the electric dipole-dipole mechanism, the Rc for energy transfer between Eu^{2+} also can be expressed by[23]

$$R_C^{\,6} = 0.63\times10^{28} Q_A / E^4 \int f_S(E) F_A(E) dE \qquad (3)$$

Where Q_A = 4.8x10^{-16}f_d is the absorption coefficient of Eu^{2+}, f_d is the oscillator strength of the transition, which is taken as 0.01 for Eu^{2+}. E is the energy of the maximum spectral overlap and $\int f_S(E)F_A(E)dE$ is the spectral overlap integral from the normalized excitation and emission spectrum of BCMSO:Eu^{2+}. The values of E and $\int f_S(E)F_A(E)dE$ were determined to be 3.048eV and 0.0363eV^{-1} from the normalized excitation and emission spectrum. Therefore, the calculated value R_c is about 15.28 Å. This result further confirms that the energy transfer mechanism between Eu^{2+} occurs via a dipole-dipole interaction.

3.3. Energy transfer mechanism of $BaCa_2MgSi_2O_8:Eu^{2+},Mn^{2+}$ phosphors

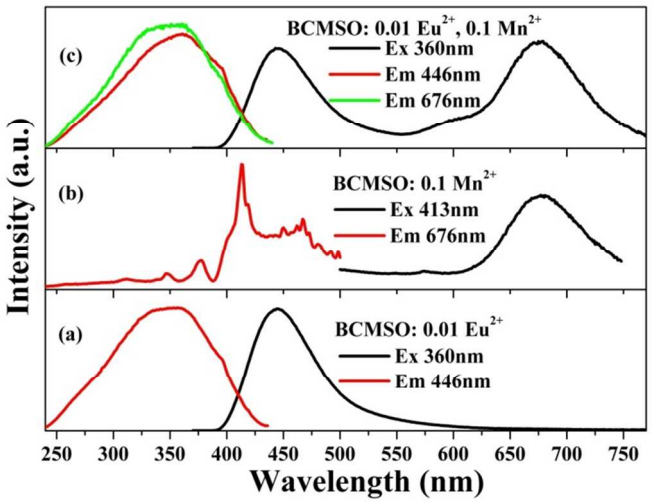

Fig. 4 PLE and PL spectra of (a)$BaCa_2MgSi_2O_8$: $0.01Eu^{2+}$, (b) $BaCa_2MgSi_2O_8$: $0.10Mn^{2+}$, and (c) $BaCa_2MgSi_2O_8$:0.01 Eu^{2+},$0.01Mn^{2+}$ phosphors.

Figure 4a and 4b show the excitation and emission spectra of BCMSO: 0.01 Eu^{2+} and BCMSO: 0.1 Mn^{2+} samples, respectively. The emission spectrum of BCMSO: 0.1 Mn^{2+} present a broad band extending from 600 to 750nm excited 413nm, peaking at 676 nm. However, the emission intensity is much weaker than that of BCMSO: 0.01 Eu^{2+} excited at 360 nm in Fig. 4a, which is due to the $^4T_1(^4G) — {}^6A_1(^6S)$ spin-forbidden transition of Mn^{2+} ions. The excitation spectrum monitored at 676 nm consists of several peaks at 346, 377, 413 and 466 nm that are in good agreement with the transitions of the Mn^{2+} ions from the ground level $^6A_1(^6S)$ to $^4E(^4D)$, $^4T_2(^4D)$, $[^4A_1(^4G),^4E(^4G)]$, and $^4T_1(^4G)$ excited levels, respectively. A significant spectral overlap between the emission band of BCMSO: 0.01 Eu^{2+} and excitation band of BCMSO: 0.1 Mn^{2+} can be seen from Fig. 4a and 4b, which demonstrates the possibility of resonance type energy transfer from Eu^{2+} to Mn^{2+} ions in this host. Figure 4c illustrate the PLE and PL spectra of the typical BCMSO:0.01 Eu^{2+}, 0.1 Mn^{2+}. It is notable that the PLE spectrum monitored with 676nm (Mn^{2+} emission) has a profile similar to that of the excitation band monitored with 446nm (Eu^{2+} emission) except for the difference of the relative intensity, revealing that the Mn^{2+} ions are essentially excited through the Eu^{2+} ions. This result also demonstrates that an efficient energy transfer from Eu^{2+} to Mn^{2+} occurs. In addition , their excitation spectra are similar to that of Eu^{2+} singly doped sample, which shows that doubly doped BCMSO can be used as blue and reddish-orange double-color-emitting phosphors in ultraviolet (UV)-pumped white LEDs. On the other hand, the emission spectrum of BCMSO: 0.01 Eu^{2+}, 0.1 Mn^{2+} phosphors under 360nm excitation includes a broad blue emission of the Eu^{2+} and the reddish-orange emission of the Mn^{2+} ions. Therefore, white-light emission can be realized by combining the emission of Eu^{2+} and Mn^{2+} ions in a single host lattice under UV light excitation by properly tuning the emission composition of the Eu^{2+} and Mn^{2+} ions through the principle of energy transfer.

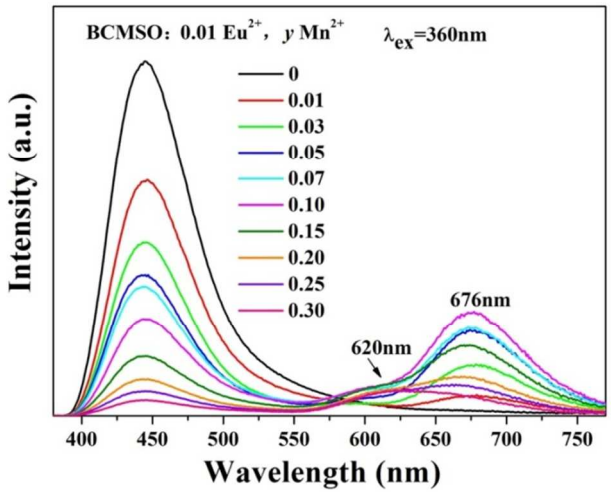

Fig. 5 PL spectra of $BaCa_2MgSi_2O_8$: 0.01 Eu^{2+}, *y* Mn^{2+} phosphors as a function of Mn^{2+} doping content (*y*).

To investigate the dependence of tunable emission on Mn^{2+} content, a series of BCMSO:0.01 Eu^{2+}, *y* Mn^{2+} (*y*=0, 0.01, 0.03, 0.05, 0.07, 0.10, 0.15, 0.20, 0.25 and 0.30) samples have been prepared. The PL spectra of BCMSO:0.01 Eu^{2+}, *y* Mn^{2+} phosphors excited at 360 nm are depicted in Fig. 5. The intensity of the Eu^{2+} emission (446 nm) decrease with an increasing doped Mn^{2+} content. In contrast, the PL spectra of the Mn^{2+} emission (676nm) increases until the maximum is reached at *y*= 0.10, and the emission intensity decreases. It is due to the Mn^{2+}-Mn^{2+} internal concentration quenching process. In addition, a broad band emission at approximately 620 nm of Mn^{2+} is observed as the concentration of Mn^{2+} increase gradually, which could be originated from the change of crystal field strength. When Mn^{2+} ions is introduced into the BCMSO host, the lattice constants *a, b, c* and *V* for samples decrease because of the ionic radius of Mn^{2+} is smaller than that of the Mg^{2+} ion. It leads to lattice distortion and further results in a larger crystal field splitting of Mn^{2+} 3d energy levels with increasing of Mn^{2+} concentration.

To observe directly the relative emission intensity variation, the intensities of Eu^{2+} and Mn^{2+} emissions are given in Fig. 6 as a function of the Mn^{2+} content. The observed variations in the Eu^{2+} and Mn^{2+} emission curves further support the occurrence of effective energy transfer from the Eu^{2+} to Mn^{2+} ions. Therefore, the Eu^{2+} to Mn^{2+} energy transfer efficiency (η_T) in the BCMSO host can be calculated by the equation: [24-25]

$$\eta_T = 1 - \frac{I_S}{I_{S0}} \qquad (4)$$

Where I_{so} is the intensity of the sensitizer (Eu^{2+}) in the absence of the activator Mn^{2+} and $I_s$is the intensity of the sensitizer in the presence of the activator. The dependence of η_T on the Mn^{2+} doping

concentration is shown in Fig. 6. It is clearly observed that the energy transfer efficiency monotonously ascends with continuous increase in Mn^{2+} concentration while the increasing rate decreases because the fixed Eu^{2+} concentration restricts the energy transfer from Eu^{2+} ions to Mn^{2+} ions. The maximum η_T value is determined to be as high as 95.5% for the BCMSO: 0.01 Eu^{2+}, 0.30 Mn^{2+} phosphor.

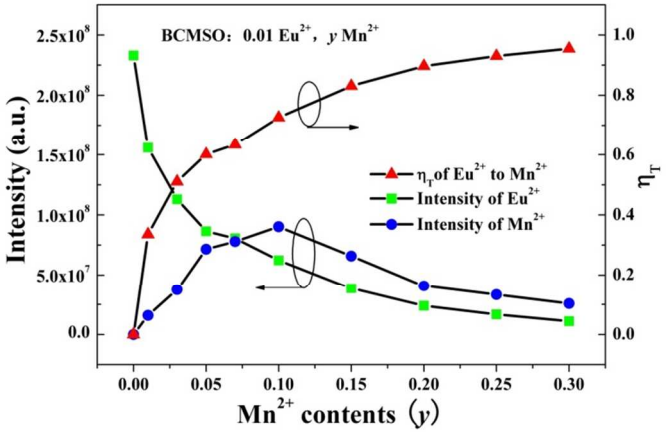

Fig. 6 Dependence of the intensity of Eu^{2+} emission, Mn^{2+} emission, and the energy transfer efficiency η_T on the Mn^{2+} contents (y) for $BaCa_2MgSi_2O_8$: 0.01 Eu^{2+}, y Mn^{2+} phosphors.

In order to well understand the energy-transfer between Eu^{2+} ions and Mn^{2+} ions in BCMSO, the decay curves of BCMSO: 0.01 Eu^{2+}, y Mn^{2+} phosphors were measured and depicted in Fig. 7 (λ_{ex}=360nm, λ_{em}=446nm). The lifetime decay curves have been analyzed by curve fitting and all the decay curves can be fitted successfully based on the following double-exponential equation: [26]

$$I(t) = I_0 + A_1 \exp(-t/\tau_1) + A_2 \exp(-t/\tau_2) \qquad (5)$$

Where I and I_0 are the luminescence intensities at times t and 0, A_1 and A_2 are fitting constants, τ_1 and τ_2 are the short and long lifetimes for the exponential components, respectively. Furthermore, the effective lifetime constant (τ*) can be calculated as

$$\tau^* = (A_1\tau_1^{\,2} + A_2\tau_2^{\,2})/(A_1\tau_1 + A_2\tau_2) \qquad (6)$$

The average decay times (τ*) were calculated to be 486.6ns, 424.1ns, 415.4ns, 389.1ns, 361.1ns and 340.8ns for BCMSO: 0.01Eu^{2+}, y Mn^{2+} with y=0, 0.05, 0.10, 0.15, 0.25 and 0.30, respectively. The decay lifetime for the Eu^{2+} ions decreases monotonically with an increase in the Mn^{2+} doping content, which is a strong evidence for the energy transfer from the Eu^{2+} to Mn^{2+} ions, and the energy transfer process may happen via resonant-type mechanism. According to the Dexter's energy transfer expression of multipolar interaction and Reisfeld's approximation, the energy transfer mechanism from Eu^{2+} to Mn^{2+} ions in this host should occur via electric multipole-multipole interaction. The following relation can be adopted: [27-29]

$$\eta_{S0}/\eta_S \propto C^{n/3} \qquad (7)$$

Where η_{so} is the intrinsic luminescence quantum efficiency of the Eu^{2+} ions, η_s is the luminescence quantum efficiency of the Eu^{2+} ions with the existence of activator (Mn^{2+}) and C is the dopant concentration of Mn^{2+}. When the value of n is 6,8 or 10, the form of the interaction corresponds to dipole-dipole (d-d), dipole-quadrupole (d-q), or quadrupole-quadrupole (q-q), respectively. In order to conduct simple assess, the value of η_{so}/η_s can be approximately estimated from the luminescence intensity ratio (I_{so}/I_s) as follows:

$$I_{S0}/I_S \propto C^{n/3} \qquad (8)$$

Where I_{so} and I_s are emission intensity of Eu^{2+} in the absence and presence of Mn^{2+}, respectively. The relationships between (I_{so}/I_s) and $C^{n/3}$ are illustrated in Fig. 8, shows that the linear dependence of the dipole-quadrupole interaction is the best one among the fitting results. This clearly indicates that the energy transfer from Eu^{2+} to Mn^{2+} follows a non-radiative dipole-quadrupole interaction. In addition, according to dipole-quadrupole interaction mechanism, the energy transfer critical distance (Rc) between Eu^{2+} and Mn^{2+} ions can be obtained from the following equation: [30-32]

$$R_C^{\,8} = 3.024\times10^{12}\,\lambda_S^2 f_q \int f_S(E)F_A(E)/E^4 dE \qquad (9)$$

Where f_q=10^{-10} is the oscillator strength of the dipole and quadrupole electrical absorption transitions for Mn^{2+}, [33] λs = 4460 Å is the wavelength of strongest intensity of Eu^{2+}, E is the energy involved in the transfer (in eV), and $\int f_S(E)F_A(E)/E^4 dE$ represents the spectral overlap between the normalized shapes of the donor Eu^{2+} emission $\int f_S(E)$ and the acceptor Mn^{2+} excitation $\int F_A(E)$, and in our case it is calculated to be about 0.01618 eV^{-5}. Therefore, the values of Rc of energy transfer from Eu^{2+} to Mn^{2+} in BCMSO are calculated to be about 9.97 Å.

RSC Advances RSCPublishing

PAPER

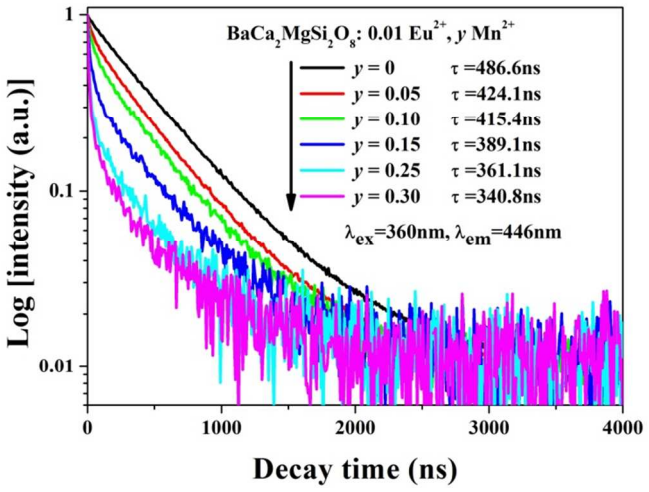

Fig. 7 Decay curves and evaluated lifetimes of Eu^{2+} emission in $BaCa_2MgSi_2O_8$: $0.01Eu^{2+}$, yMn^{2+} phosphors under excitation at 360 nm, monitored at 446 nm.

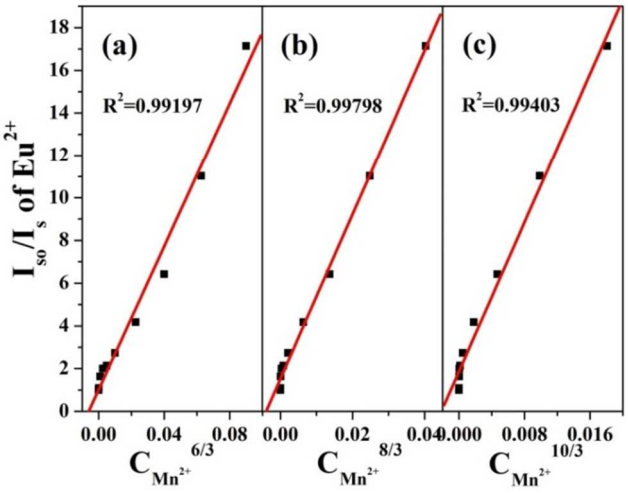

Fig. 8 Dependence of I_{S0}/I_S of Eu^{2+} on (a) $C^{6/3}$,(b) $C^{8/3}$ and (c) $C^{10/3}$ in the $BaCa_2MgSi_2O_8$:$0.01Eu^{2+}$, *y* Mn^{2+} phosphors.

Figure 9 and Table 1 show the CIE chromaticity diagram and chromaticity coordinates (x, y) of the single-phase emission-tunable phosphor BCMSO:$0.01Eu^{2+}$, *y* Mn^{2+} under 360 nm excitation. The chromaticity coordinates (x, y) for BCMSO:$0.01Eu^{2+}$, *y* Mn^{2+} phosphors were measured to be (0.1650, 0.1134), (0.1741,0.1210), (0.1920,0.1158), (0.2249,0.1345), (0.2479,0.1567), (0.2797,0.1804), (0.3156,0.2012), (0.3384,0.2176), (0.3674,0.2374) eventually to (0.4100,0.2671) with *y*= 0, 0.01, 0.03, 0.05, 0.07, 0.10, 0.15, 0.20, 0.25 and 0.30. These results indicate that the color can be tuned from blue (solely $0.01Eu^{2+}$, point 1) through white-light ($0.01Eu^{2+}$/ $0.20Mn^{2+}$, point 8) and eventually to red ($0.01Eu^{2+}$/$0.30Mn^{2+}$, point 10) in the visible spectral region by systematically adjusting the relative Mn^{2+} dopant concentrations. The insets of Fig. 9 show photographs of BCMSO:$0.01Eu^{2+}$, *y* Mn^{2+} phosphors with different Mn^{2+} contents *y* in a 365 nm UV lamp box. Thus, the emitting is tunable in a large color gamut by adjusting the doping content of Mn^{2+} ions. In particular, a white light emission with CIE coordinate of (0.3384,0.2176) can be obtained by combining the emission of Eu^{2+} and Mn^{2+} in a single host, as shown in point 8 (white region) in Fig. 9.

In order to further verify the occupancy of the cation sites, the following equation (10) has been used to build up the relationship between the coordination environment and emission peaks, which is proposed by Van Uitert and successfully used to explain many structure–property relationship studies in Eu^{2+} doped systems.

$$E = Q\left[1-\left(\frac{V}{4}\right)^{\frac{1}{V}} 10^{-\frac{n\times Ea\times r}{80}}\right] \qquad (10)$$

where E is the position of the rare-earth ion emission peak (cm^{-1}), *Q* represents the position in energy for the lower d-band edge for the free ion (*Q* = 34000 cm^{-1} for Eu^{2+}), V is the valence of the "active" cation (*V* = 2 for Eu^{2+}), n is the number of anions in the immediate shell around the "active" cation, and r is the radius of the host cation occupied by the Eu^{2+} ion (Å). *Ea* is the electron affinity of the atoms that form anions (eV), which is different when Eu^{2+} is introduced into different anion complexes with various coordination numbers. Here, *Ea* is approximately determined as 2.5 *eV*, as reported in other systems. According to equation (10), the crystallographically independent Ba^{2+} and Ca^{2+} cation sites in $BaCa_2MgSi_2O_8$ provide different crystal fields for the rare-earth ion Eu^{2+} emission. In $BaCa_2MgSi_2O_8$, the Ba atom is twelve-fold coordinated by six O2 and six O1 atoms, the distances of Ba-O2 and Ba-O1 are 2.7721 Å and 3.1240 Å , respectively. Among them, Ba-O2 bond is extremely short compared with Ba-O1. A closeness of a cation and the ligand increases the ligand field strength. Therefore, the six O2 act as a dominant role for the ligand field strength. The Ca atom is seven-fold coordinated by oxygen atoms. All three of these conditions were calculated based on equation (10) respectively, and the results are listed in Table 2.

In order to further determine the absolute quantum efficiency of photo-conversion for these novel phosphors, herein we have used integrated sphere method for the measurements of optical absorbance (A) and quantum efficiency (Φ) of phosphor samples. The absorbance and quantum efficiencies of BCMSO:1%Eu^{2+}, BCMSO:1%Eu^{2+}, 10%Mn^{2+} and commercial blue-emitting phosphor – $BaMgAl_{10}O_{17}$:Eu^{2+} (Kasei-661) are calculated by using these following equations:

$$A = \frac{L_0(\lambda) - L_i(\lambda)}{L_0(\lambda)} \qquad (11)$$

where $L_0(\lambda)$ is the integrated excitation profile when the sample is diffusely illuminated by the integrated sphere's surface; $L_i(\lambda)$ is the integrated excitation profile when the sample is directly excited by the incident beam. Furthermore, quantum efficiency (Φ) of these phosphors can be calculated by

$$\Phi = \frac{E_i(\lambda) - (1-A) \bullet E_0(\lambda)}{L_e(\lambda) \bullet A} \qquad (12),$$

where $E_i(\lambda)$ is the integrated luminescence of the powder upon direct excitation, and $E_o(\lambda)$ is the integrated luminescence of the powder excited by indirect illumination from the sphere. The term $L_e(\lambda)$ is the integrated excitation profile obtained from the empty integrated sphere (without the sample present). The absorbance of BCMSO:1%Eu^{2+}, BCMSO:1%Eu^{2+}, 20%Mn^{2+} and $BaMgAl_{10}O_{17}$:Eu^{2+} phosphors were found to be 81.1, 68.7 and 68.5 at the excitation wavelength of 360 nm, and the corresponding QE was found to be 93.5%, 53.6%, and 16.5%, respectively. The internal quantum efficiency of BCMSO:1%Eu^{2+} is about 57% of commodity. We believe the quantum efficiency would be enhanced by optimizing the parameters, such as fluxes, starting materials and synthetic arts.

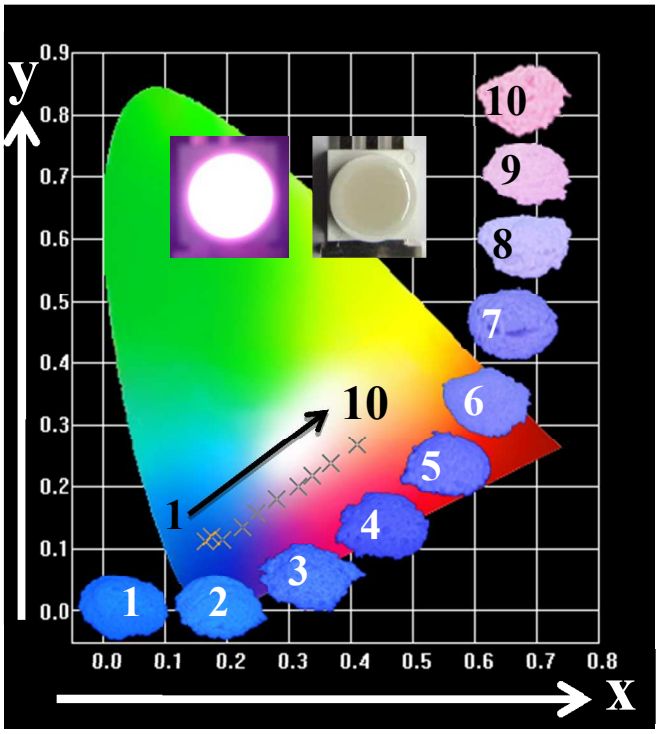

Fig. 9 CIE coordinates of $BaCa_2MgSi_2O_8$:0.01Eu^{2+}, y Mn^{2+} phosphors (y = 0, 0.01, 0.03, 0.05, 0.07, 0.10, 0.15, 0.20, 0.25 and 0.30). Numbers shown in the figure correspond to those described in Table 1. The insets show the phosphor images with different Mn^{2+} doping concentration excited at 365 nm in the UV box and the LED package of 380 nm chip and $BaCa_2MgSi_2O_8$:0.01Eu^{2+}, 0.20Mn^{2+} phosphor.

Table 1 The CIE coordinates of $BaCa_2MgSi_2O_8$:0.01Eu^{2+}, y Mn^{2+} phosphors (y = 0, 0.01, 0.03, 0.05, 0.07, 0.10, 0.15, 0.20, 0.25and 0.30) excited at 360 nm.

No.	Compositions	CIE (x, y)
1	$BaCa_2MgSi_2O_8$:0.01Eu	(0.1650, 0.1134)
2	$BaCa_2MgSi_2O_8$:0.01Eu, 0.01Mn	(0.1741, 0.1210)
3	$BaCa_2MgSi_2O_8$:0.01Eu, 0.03Mn	(0.1920, 0.1158)
4	$BaCa_2MgSi_2O_8$:0.01Eu, 0.05Mn	(0.2249, 0.1345)
5	$BaCa_2MgSi_2O_8$:0.01Eu, 0.07Mn	(0.2479, 0.1567)
6	$BaCa_2MgSi_2O_8$:0.01Eu, 0.10Mn	(0.2797, 0.1804)
7	$BaCa_2MgSi_2O_8$:0.01Eu, 0.15 Mn	(0.3156, 0.2012)
8	$BaCa_2MgSi_2O_8$:0.01Eu, 0.20 Mn	(0.3384, 0.2176)
9	$BaCa_2MgSi_2O_8$:0.01Eu, 0.25 Mn	(0.3674, 0.2374)
10	$BaCa_2MgSi_2O_8$:0.01Eu, 0.30 Mn	(0.4100, 0.2671)

RSC Advances RSCPublishing

PAPER

Table 2 The calculated results of the Eu^{2+} emission peak position for Ba^{2+} and Ca^{2+} occupancy cation sites respectively based on equation (10).

Occupancy site	Ea(eV)	n	r(Å)	E(calculated) (cm^{-1})	λ(calculated) (nm)	λ(measured) (nm)
Ba^{2+}	2.5	6	1.35	20577.33	486	(390-600)
Ba^{2+}	2.5	12	1.61	20577.33	357	peak at 446
Ca^{2+}	2.5	7	1.06	19904.23	502	

4. Conclusions

This study reports the synthesis of a novel single-phase white light-emitting UV LED phosphors - BCMSO:Eu^{2+}, Mn^{2+} using a solid state reaction. The energy transfer from Eu^{2+} to Mn^{2+} in BCMSO host was a resonant type via a non-radiative dipole-quadrupole mechanism. A white light could be generated by co-doping Eu^{2+} and Mn^{2+} ions. The optimal-composition for with light is BCMSO:0.01Eu^{2+}, 0.2Mn^{2+}, which gives the CIE coordinates of (0.3384,0.2176). These results indicate that BCMSO:Eu^{2+}, Mn^{2+} phosphor could be a promising single-composition phosphor for application involving white-light UV LEDs.

Acknowledgments

This research was supported by the National Science Council of Taiwan under contract No. NSC-102-2221-E-033-050-MY2 and the Research Fund for the Doctoral Program of Higher Education of China (RFDP) (No.20136101110017）.

Notes and references

[a] *National Key Laboratory of Photoelectric Technology and Functional Materials (Culture Base) in Shaanxi Province, Institute of Photonics & Photon-Technology, Northwest University, Xi'an 710069, China. E-mail:guocf@nwu.edu.cn*

[b] *Department of Chemical Engineering, Chung Yuan Christian University, Chung Li, Taiwan, R.O.C. Fax: +886-3-2654199; Tel: +886-3-2654140;E-mail: WRLiu1203@gmail.com*

† Electronic Supplementary Information (ESI) available: [details of any supplementary information available should be included here]. See DOI: 10.1039/b000000x/

‡ *Corresponding authors: both Wei-Ren Liu and Chong-Feng Guo are corresponding authors.

1 S. Nakamura, T. Mukai and M. Senoh, *Appl. Phys. Lett.*, 1994, **64**, 1687-1689.

2 W. B. Im, Y. I. Kim, N. N. Fellows, H. Masui, G. A. Hirata, S. P. DenBaars and R. Seshadri, *Appl. Phys. Lett.*, 2008, **93**, 0919051.

3 T. Nishida, T. Ban, N. Kobayashi, *Appl. Phys. Lett.*, 2003, **82**, 3817-3819.

4 S. Muthu, F. J. P. Schuurmans and M. D. Pashley, *IEEE J. Sel. Top. Quantum Electron.*, 2002, **8**, 333-338.

5 S. Lee and S. Y. J. Seo, *Electro. chem. Soc.*, 2002, **149**, 85-88.

6 Z. Hao, J. Zhang, X.Zhang, X. Sun, Y. Luo, S. Lu and X. Wang, *Appl. Phys. Lett.*, 2007, **90**, 261113.

7 J. S. Kim, P. E. Jeon, Y. H. Park, J. C. Choi, H. L. Park, G. C. Kim and T. W.Kim, *Appl. Phys. Lett.*, 2004, **85**, 3696-3698.

8 W. R. Liu, C. H. Huang, C. W.Yeh, J. C. Tsai, Y. C. Chiu, Y. T. Yeh and R. S. Liu, *Inorg. Chem.*, 2012, **51**, 9636-9641.

9 W. Lü, Z. Hao, X. Zhang, Y. Luo, X. Wang and J. Zhang, *Inorg. Chem.*, 2011, **50**, 7846-7851.

10 J. Zhang, Y. Wang, F. Zhang and Y. J. Huang, *Electrochem. Soc.*, 2011, **158**, 102-110.

11 Z. G. Xia, Y. Y. Zhang, M. S. Molokeev and V. V. Atuchin, *J. Phys. Chem. C*, 2013, **117**, 20847-20854.

12 Y. Yonesaki, T. Takei, N. Kumada and N. Kinomura, *J. Solid State Chem.*, 2009, **182**, 547-554.

13 C. H. Park, T. H. Kim, Y. Yonesaki and N. Kumada, *J. Solid State Chem.*, 2011, **184**, 1566-1570.

14 Y. Yonesaki, T. Takei, N. Kumada and N. Kinomura, *J. Lumin.*, 2008, **128**, 1507-1514.

15 D. J. Hou, C. M. Liu, X. M. Ding, X. J. Kuang, H. B. Liang, S. S. Sun, Y. Huang and Y. Tao, *J. Mater. Chem. C*, 2013, **1**, 493-499.

16 D. J. Hou, W. Chen, X. M. Ding, H. B. Liang, L. R. Zheng and J. Zhang, *ECS J. Solid State Sci. Technol.*, 2013, **2**, R79-R81.

17 W. Lü, Y. C. Jia, W. Z. Lv, Q. Zhao and H. P. You, *RSC Adv.*, 2013, **3**, 20619-20624.

18 I. T. Ivanov and G. N. Kirov, *Inorg. Mater.*, 1977, **13**, 470.

19 R. D. Shannon, Acta. Crystallogr., *Sect. A: Cryst. Phys., Diffr., Theor. Gen. Crystallogr.*, 1976, **32**, 751-767.

20 H. Zhang, T. Horikawa, H. Hanzawa, A. Hamaguchi and K. I. Machida, *J. Electrochem. Soc.*, 2007, **154**, 59-61.
21 (a) L. Ozawa and P. M. Jaffe, *J. Electrochem. Soc.*, 1971, **118**, 1678-1679; (b) L. G. Van Uitert, *J. Electrochem. Soc.*, 1976, **114**, 1048-1053.
22 G. J. Blasse, *Solid State Chem.*, 1986, **62**, 207-211.
23 D. L. J. Dexter, *J. Chem. Phys.*, 1953, **21**, 836-850.
24 P. I. Paulose, G. Jose, V. Thomas, N. V. Unnikrishnan and M. K. R. Warrier, *J. Phys. Chem. Solid*, 2003, **64**, 841-846.
25 C. F. Guo, X. Ding, L. Luan and Y. Xu, *Sensor Actuat B*, 2010, **143**, 712-715.
26 C. H. Huang and T. M. Chen, *J. Phys. Chem. C*, 2011, **115**, 2349-2355.
27 D. L. Dexter and J. H. Schulman. *J. Chem. Phys.,* 1954, **22**, 1063-1070.
28 W. R. Liu, C. H. Huang, C. W.Yeh, J. C. Tsai, Y. C. Chiu, Y. T. Yeh and R. S. Liu, *RSC Adv.*, 2013, **3**, 9023-9028.
29 C. F. Guo, Z. Yang, J. Yu and J. H. Jeong, *Appl Phys. A*, 2012, **108**, 569-576.
30 N. Guo, Y. J. Huang, H. P. You, M. Yang, Y. H. Song, K. Liu and Y. H. Zheng, *Inorg. Chem.*, 2010, **49**, 10907-10913.
31 K. Li, D. L. Geng, M. M. Shang, Y. Zhang, H. Z. Lian and J. Lin, *J. Phys.Chem. C*, 2014, **118**, 2686-2692.
32 C. H. Huang, T. S. Chan, W. R. Liu, D. Y. Wang, Y. C. Chiu, Y. T. Yeha and T. M. Chen, *J. Mater. Chem.*, 2012, **22**, 20210-20216.
33 K. S. Sohn, E. S. Park, C. H. Kim and H. D. Park, *J. Electrochem. Soc.*, 2000, **147**, 4368-4373.

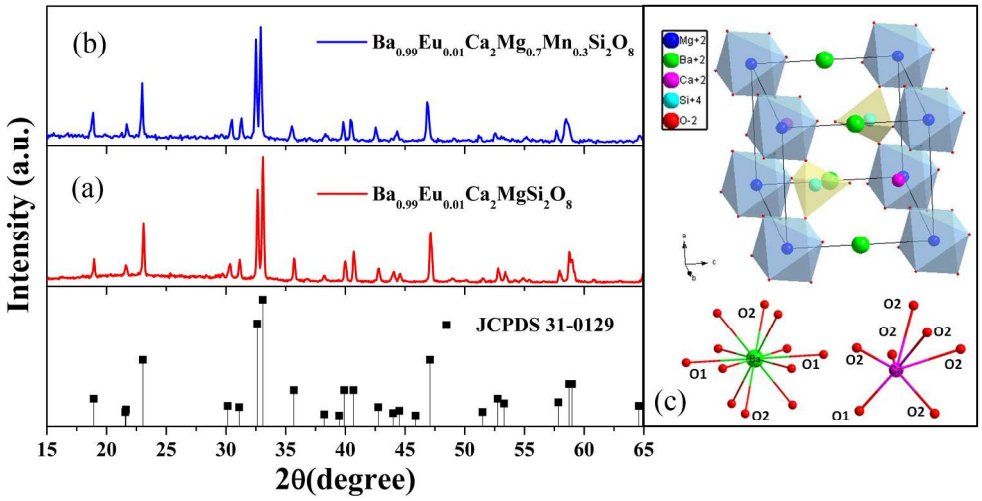

Powder XRD patterns of (a) Ba0.99Eu0.01Ca2MgSi2O8, (b) Ba0.99Eu0.01Ca2Mg0.7Mn0.3Si2O8 and (c) the crystal structure of BaCa2MgSi2O8 and coordination environment of Ba and Ca atoms in BaCa2MgSi2O8.
443x243mm (144 x 144 DPI)

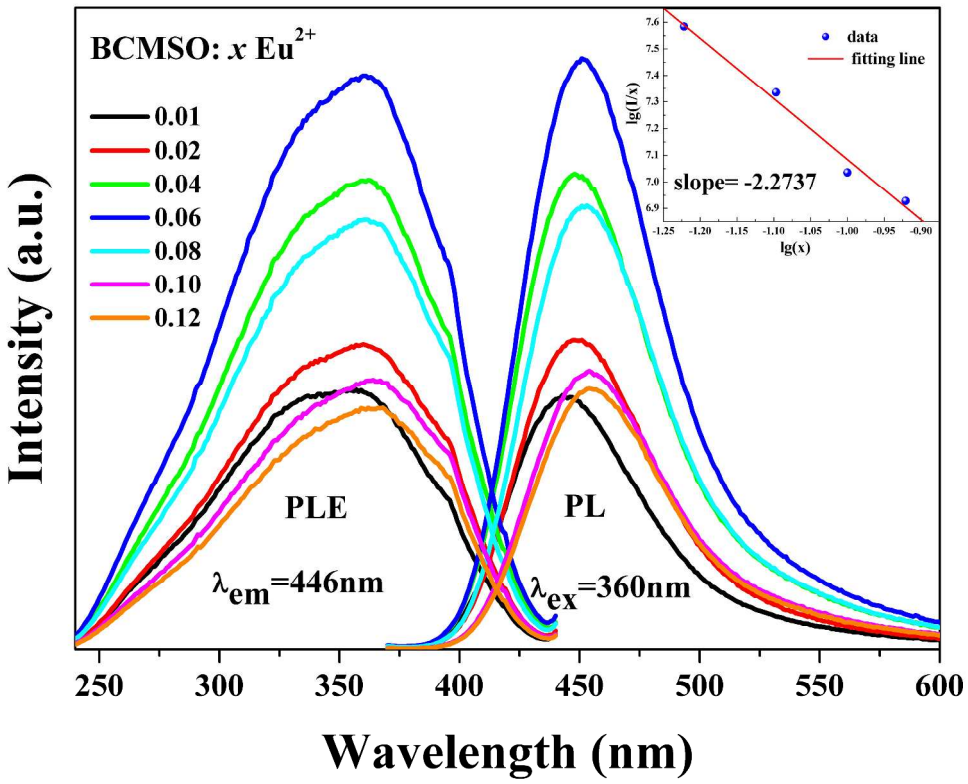

PLE and PL spectra of BaCa2MgSi2O8:xEu2+ phosphors (x=0.01, 0.02, 0.04, 0.06, 0.08, 0.10, 0.12), and the inset shows the fitting of log(I/x) vs log(x) in BaCa2MgSi2O8:x Eu2+ phosphors.
908x721mm (144 x 144 DPI)

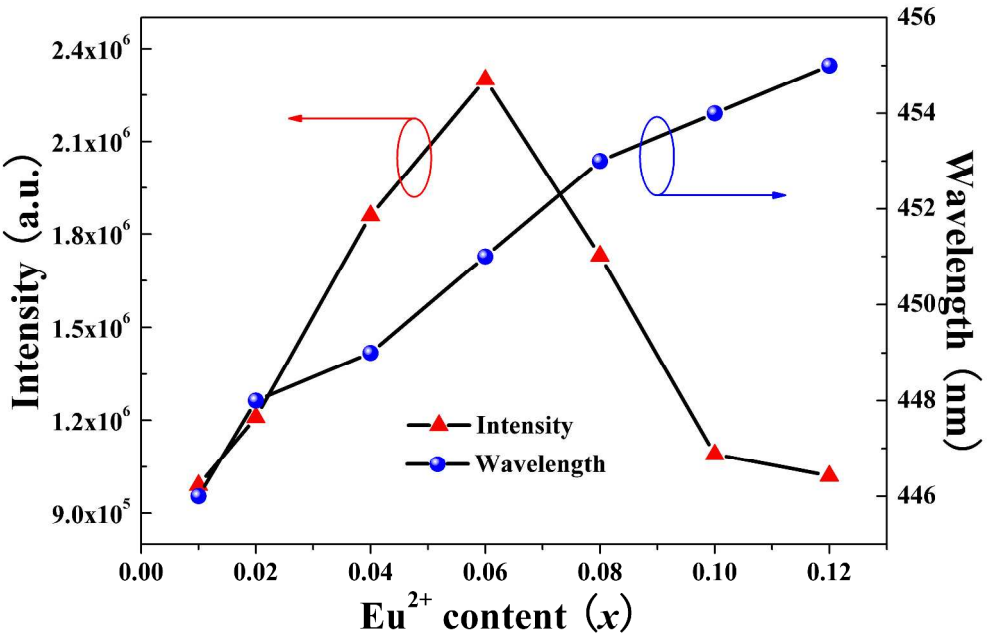

The intensity and wavelength dependence of Eu2+ emission on the Eu2+ content x in samples BaCa2MgSi2O8:x Eu2+.
1136x746mm (144 x 144 DPI)

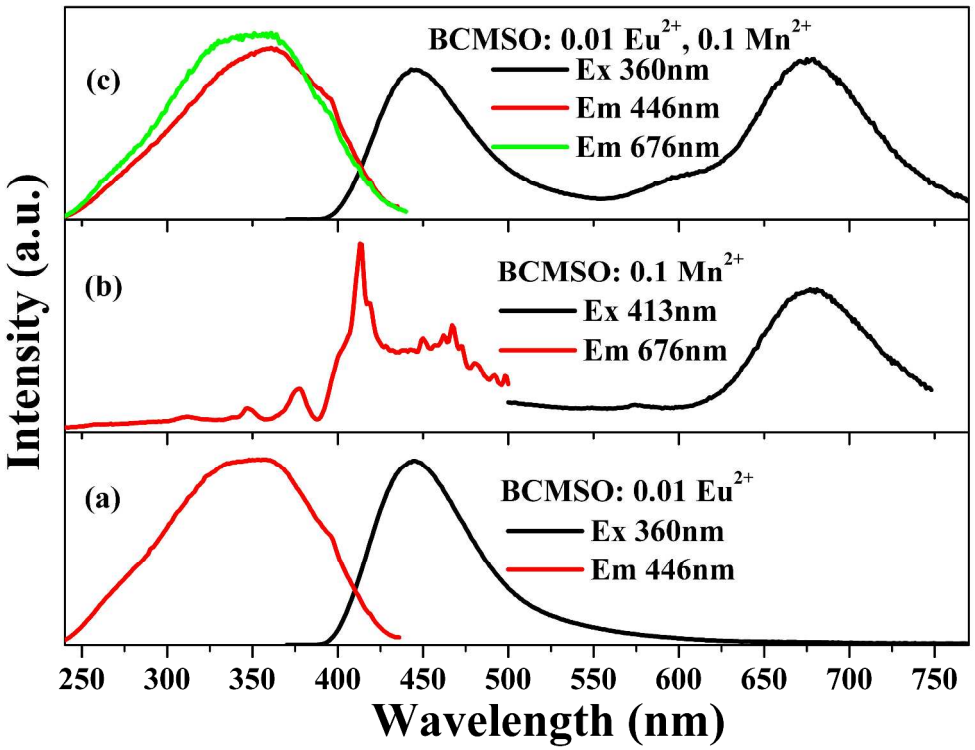

PLE and PL spectra of (a) BaCa2MgSi2O8: 0.10Mn2+, (b) BaCa2MgSi2O8: 0.01Eu2+, and (c) BaCa2MgSi2O8:0.01 Eu2+,0.01Mn2+ phosphors.
1028x785mm (144 x 144 DPI)

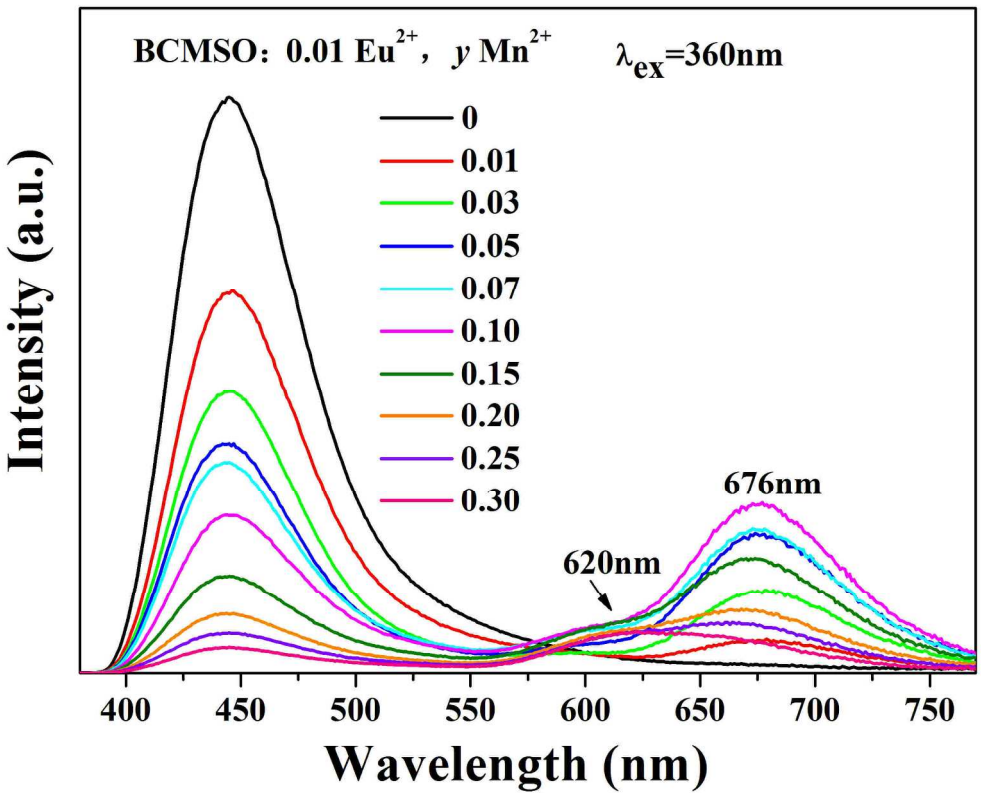

PL spectra of BaCa2MgSi2O8: 0.01 Eu2+, y Mn2+ phosphors as a function of Mn2+ doping content (y).
472x382mm (144 x 144 DPI)

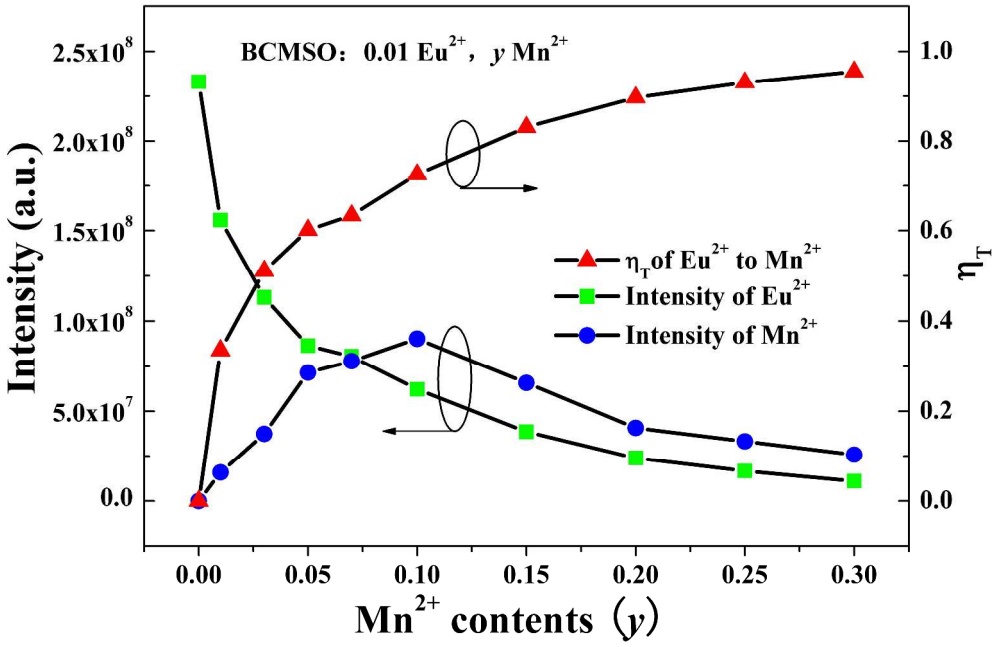

Dependence of the intensity of Eu2+ emission, Mn2+ emission, and the energy transfer efficiency ηT on the Mn2+ contents (y) for BaCa2MgSi2O8: 0.01 Eu2+, y Mn2+ phosphors.
1108x728mm (144 x 144 DPI)

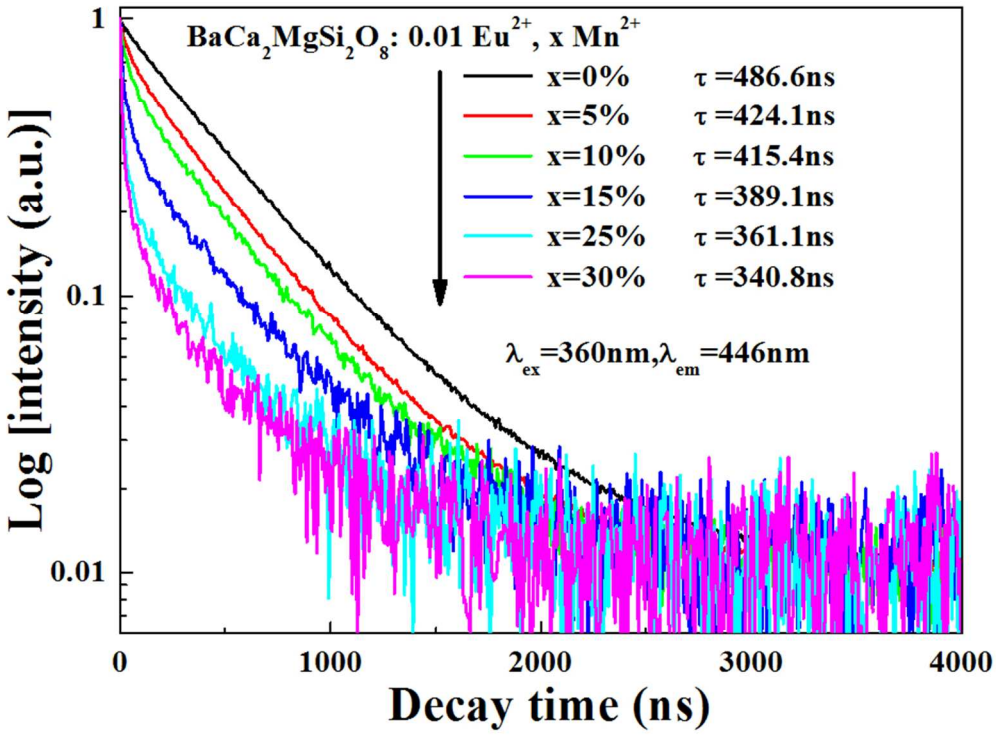

Decay curves and evaluated lifetimes of Eu2+ emission in BaCa2MgSi2O8: 0.01Eu2+, yMn2+ phosphors under excitation at 360 nm, monitored at 446 nm.
165x122mm (144 x 144 DPI)

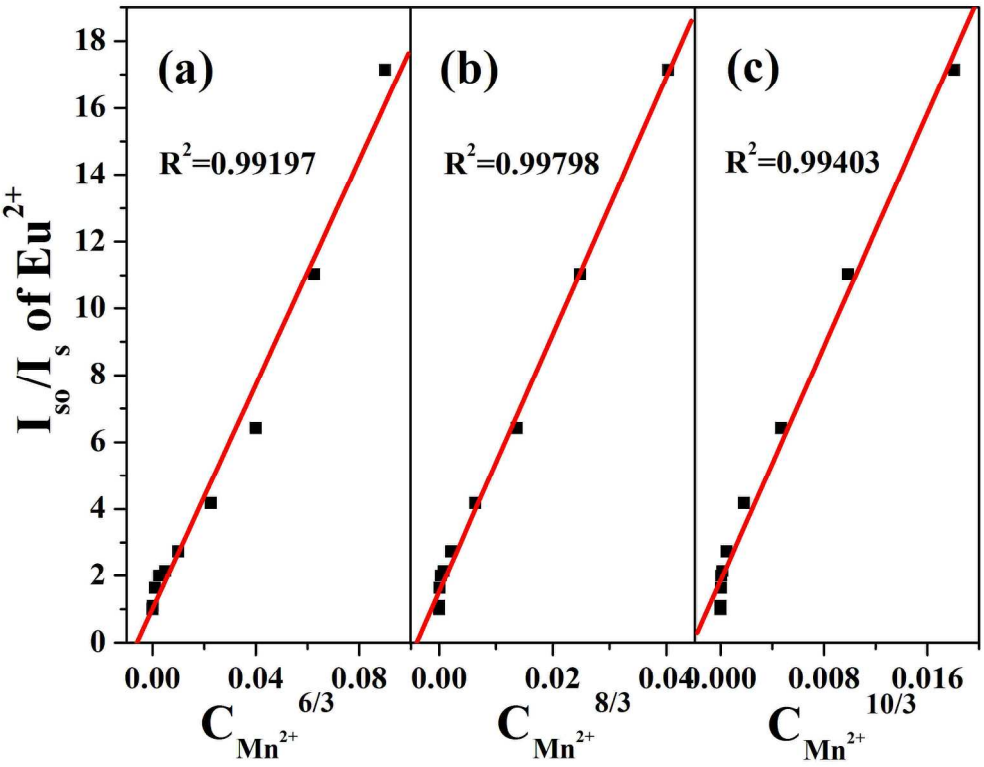

Dependence of IS0/IS of Eu2+ on (a) C6/3 ,(b) C8/3 and (c) C10/3 in the BaCa2MgSi2O8:0.01Eu2+, y Mn2+ phosphors.
498x389mm (144 x 144 DPI)

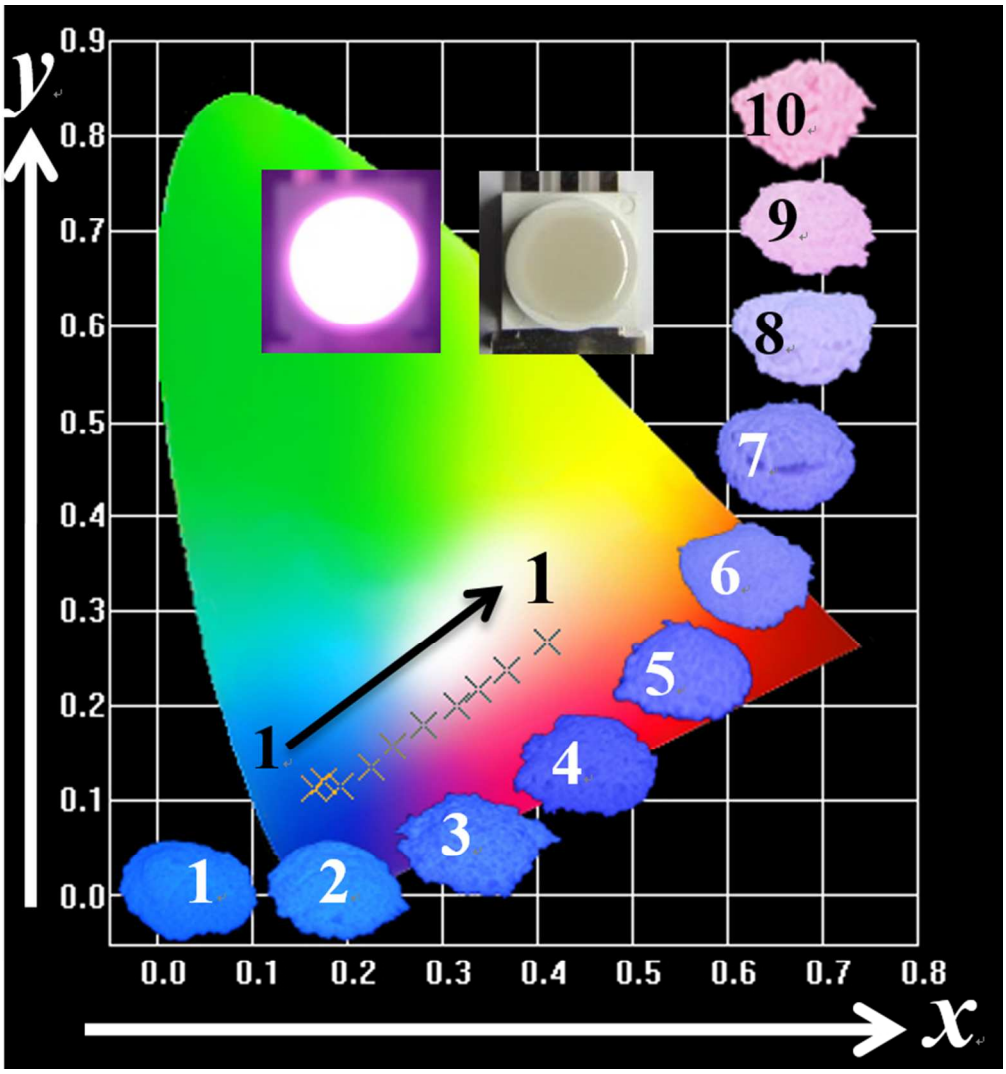

CIE coordinates of BaCa2MgSi2O8:0.01Eu2+, y Mn2+ phosphors (y = 0, 0.01, 0.03, 0.05, 0.07, 0.10, 0.15, 0.20, 0.25and 0.30). Numbers shown in the figure correspond to those described in Table 1. The insets show the phosphor images with different Mn2+ doping concentration excited at 365 nm in the UV box and the LED package of 380 nm chip and BaCa2MgSi2O8:0.01Eu2+, 0.20Mn2+ phosphor.
146x156mm (144 x 144 DPI)

Table of Contents Graphic & Summary

Zheng Yang, Pin-Chun Lin, Chong-Feng Guo and Wei-Ren Liu

RSC Advances **2015**, *xx*, XXXX

A color-tunable $BaCa_2MgSi_2O_8$:1%Eu^{2+}, 20%Mn^{2+} phosphor demonstrate a CIE coordinates of (0.3384, 0.2176) and CRI of 82. The results indicate that as-synthesized phosphor could be a single-phased and white-emitting phosphor for n-UV LEDs.

Color-tunable luminescence and energy transfer properties of Eu^{2+} and Mn^{2+}-activated $BaCa_2MgSi_2O_8$ phosphor for ultraviolet light-emitting diodes